Radiative quenching of He(2 ^1S) induced by collisions with ground-state helium atoms

B. Zygelman and A. Dalgarno
Harvard-Smithsonian Center for Astrophysics, 60 Garden Street, Cambridge, Massachusetts 02138
(Received 11 February 1988)

The semiclassical, optical potential, and quantal distorted wave theories of collision-induced radiative quenching are discussed and the relationships between them are presented. The three procedures are applied to the calculation of the cross sections at thermal collision energies of the process $He(2\,^1S)+He(1\,^1S)\rightarrow He(1\,^1S)+He(1\,^1S)+h\nu$. Several choices of the potential energy curves of the excited $A\,^1\Sigma_u^+$ state of the $^4He_2$ molecule are employed. The accuracy of the semiclassical and optical potential methods is assessed by comparison with the quantum-mechanical theory. It is shown that the cross sections are sensitive to the barrier in the $A\,^1\Sigma_u^+$ potential but the major uncertainty in the predicted cross sections lies in the adopted transition dipole moment.

I. INTRODUCTION

The cross section for the quenching of metastable helium by ground-state helium atoms

$$He(2\,^1S)+He(1\,^1S)\rightarrow He(1\,^1S)+He(1\,^1S)+h\nu \qquad (1)$$

was measured at thermal energies by Phelps, by Bartell Hurst, and Wagner, and by Payne *et al.*[1] who obtained a mean value of 3×10^{-20} cm^2. The measured value is consistent with theoretical semiclassical calculations by Browne, Allison, and Dalgarno[2] though because of the sensitivity of the thermal cross sections to the height of the barrier[3] that exists in the potential energy curve of the $A\,^1\Sigma_u^+$ state of He_2 along which the atoms initially approach the calculations have limited accuracy. Subsequently many studies have been carried out of the potential energy curve of the $A\,^1\Sigma_u^+$ state[4-8] and reliable estimates of the barrier height have been made.

Measurements[9] are in progress to determine the quenching cross sections at energies up to 400 meV. We report here the calculation of the cross sections using an improved potential energy curve in a semiclassical theory, a local optical potential theory and a fully quantum-mechanical theory of the process. We show formally the relationships between the three theories.

II. FORMALISM

In the center of mass frame of the nuclei, the Hamiltonian for the system is given by

$$H=-\frac{1}{2\mu}\nabla_R^2+H_{el}(\mathbf{R},\mathbf{r})+H_{rad}+H_{int}\ , \qquad (2)$$

where μ is the reduced mass. ∇_R is the gradient operator for the relative nuclear motion. $H_{el}(\mathbf{R},\mathbf{r})$ is the fixed-nuclei Hamiltonian for the electrons, whose coordinates are collectively labeled by the vector $\mathbf{r}$, H_{rad} is the Hamiltonian for the radiation field, and H_{int} is the radiation-matter coupling. We approximate H_{int} by including the coupling with electrons only, and using the dipole approximation. In the length gauge we have

$$H_{int}=-\sum_j \mathbf{r}_j\cdot\mathbf{E}\ ,$$
$$\mathbf{E}=i\sum_{\kappa\alpha}\left[\frac{2\pi c\kappa}{V}\right]^{1/2}\hat{\epsilon}_{\kappa\alpha}(a_{\kappa\alpha}-a_{\kappa\alpha}^\dagger)\ , \qquad (3)$$

where $a_{\kappa\alpha}, a_{\kappa\alpha}^\dagger$ are the destruction and creation operators for a photon of momentum $\hbar\kappa$ and polarization α, respectively. $\hat{\epsilon}_{\kappa\alpha}$ is the polarization vector, and V is the normalization volume. We regard the process as a transition induced by the radiation field from the $A\,^1\Sigma_u^+$ state of the He_2 molecule formed by the approaching atoms to the $X\,^1\Sigma_g^+$ state in which the atoms separate. We write for the system wave function

$$|\Psi\rangle=F_a(\mathbf{R})\chi_a(\mathbf{R},\mathbf{r})\,|0\rangle+\sum_{\kappa\alpha}F_{\kappa\alpha}(\mathbf{R})\chi_b(\mathbf{R},\mathbf{r})\,|\kappa\alpha\rangle\ , \qquad (4)$$

where $\chi_a(\mathbf{R},\mathbf{r})$ and $\chi_b(\mathbf{R},\mathbf{r})$ are eigenstates of the fixed-nuclei Hamiltonian H_{el}, corresponding to the $A\,^1\Sigma_u^+$ and $X\,^1\Sigma_g^+$ Born-Oppenheimer states, respectively, in a body-fixed frame, $F_a(\mathbf{R})$ and $F_{\kappa\alpha}(\mathbf{R})$ are the amplitudes for the relative nuclear motion, and $|0\rangle$ and $|\kappa\alpha\rangle$ are the kets for the photon vacuum and single-photon states. The ansatz (4) is valid at low collision velocities where the coupling to other channels is negligible. If nonadiabatic effects are ignored the amplitudes $F_a(\mathbf{R})$ and $F_{\kappa\alpha}(\mathbf{R})$ obey the coupled equations

$$\left[\frac{-1}{2\mu}\nabla_R^2+V_a(R)-E\right]F_a(\mathbf{R})=\sum_{\kappa\alpha}F_{\kappa\alpha}(\mathbf{R})U_{\kappa\alpha}(\mathbf{R})\ , \qquad (5a)$$

$$\left[\frac{-1}{2\mu}\nabla_R^2+V_b(R)+\hbar\omega-E\right]F_{\kappa\alpha}(\mathbf{R})=F_a(\mathbf{R})U_{\kappa\alpha}^\dagger(\mathbf{R})\ , \qquad (5b)$$

where

$$U_{\kappa\alpha}(\mathbf{R})=-i\left[\frac{2\pi c\kappa}{V}\right]^{1/2}D(R)\hat{\mathbf{R}}\cdot\hat{\epsilon}_{\kappa\alpha} \qquad (5c)$$

and $V_a(R), V_b(R)$ are the potential energy curves of the $A\,^1\Sigma_u^+$ and $X\,^1\Sigma_g^+$ states respectively. $D(R)$ is the radial transition dipole moment between them. E is the initial energy of relative motion, and ω is the angular frequency of the emitted photon. We rewrite (5b) as

$$F_{\kappa\alpha}(\mathbf{R})=\int d^3R' G^+(\mathbf{R},\mathbf{R}')F_a(\mathbf{R}')U^\dagger_{\kappa\alpha}(\mathbf{R}')\ , \tag{6}$$

where $G^+(\mathbf{R},\mathbf{R}')$ is a retarded Green's function which obeys the equation

$$\left[\frac{-1}{2\mu}\nabla_R^2+V_b(R)+\hbar\omega-E\right]G^+(\mathbf{R},\mathbf{R}')=\delta^3(\mathbf{R}-\mathbf{R}') \tag{7}$$

and satisfies the retarded boundary condition so that $F_{\kappa\alpha}$ contains only outgoing waves in the limit as $R\rightarrow\infty$. It is convenient to express this Green's function as a sum over partial waves. Since V_b contains no bound states we get

$$G^+(\mathbf{R},\mathbf{R}')=\frac{\pi\mu}{k_b}\sum_{l=0}^{\infty}\sum_{m=-l}^{m=l}Y_{lm}(\theta,\phi)Y^*_{lm}(\theta',\phi')\times\frac{f_l(k_bR_<)g_l^+(k_bR_>)}{RR'}\ , \tag{8}$$

where $Y_{lm}(\theta,\phi)$ are spherical harmonics. $f_l(kR)$ is a regular solution of the homogeneous radial equation

$$\left[\frac{d^2}{dR^2}-\frac{l(l+1)}{R^2}-2\mu[V_b(R)-V_b(\infty)]+k^2\right]f_l(kR)=0\ , \tag{9a}$$

$$k_b\equiv\sqrt{2\mu[E-\hbar\omega-V_b(\infty)]}\ ,$$

$g_l^+(kR)$ is the irregular solution with the boundary conditions at large R,

$$f_l(kR)\sim\left[\frac{2}{\pi}\right]^{1/2}\sin\left[kR-\frac{l\pi}{2}+\delta_l(b)\right]\ ,$$
$$g_l^+(kR)\sim\left[\frac{2}{\pi}\right]^{1/2}\exp i\left[kR-\frac{l\pi}{2}+\delta_l(b)\right]\ , \tag{9b}$$

and $\delta_l(b)$ is the phase shift. The total wave function (4) must be symmetric under the interchange of the He nuclei so that $F_a(\mathbf{R})=-F_a(-\mathbf{R})$, and $F_{\kappa\alpha}(\mathbf{R})=F_{\kappa\alpha}(-\mathbf{R})$, where we have used the fact that the $A\,^1\Sigma_u^+$ state is antisymmetric and the $X\,^1\Sigma_g^+$ symmetric under nuclear interchange. We now recognize that the interaction with the radiation field is weak and solve equations (5a) and (5b) in the distorted wave approximation. Then $F_a(\mathbf{R})$ is the solution of (5a) with the coupling term taken equal to zero and we may express it in the form

$$F_a(\mathbf{R})=\sum_{J=1}^{\infty}P_J(\cos\theta)(2J+1)i^J\sqrt{\pi}\times\exp[i\delta_J(a)]\frac{s_J(k_aR)}{k_aR}\ ,$$
$$k_a\equiv\sqrt{2\mu[E-V_a(\infty)]}, \tag{10a}$$

where $s_J(kR)$ is the regular solution of the homogeneous radial equation, with phase shift $\delta_J(a)$, obtained from Eq. (5a). The summation over the partial waves in (10a) is restricted to odd values of J in order to insure the correct symmetry for $F_a(\mathbf{R})$. The asymptotic form for (10a) is

$$F_a(\mathbf{R})\sim\frac{1}{\sqrt{2}}\left[e^{ik_az}-e^{-ik_az}+[f(\theta,\phi)-f(\theta-\pi,\phi+\pi)]\frac{e^{ik_aR}}{R}\right]\ . \tag{10b}$$

Inserting (10a) and (8) into (6) we get the asymptotic form for (6)

$$F_{\kappa\alpha}(\mathbf{R})\sim\frac{\exp(ik_bR)}{R}f_{\kappa\alpha}(\theta,\phi)\ , \tag{11a}$$

where

$$f_{\kappa\alpha}(\theta,\phi)=\sum_{lm}Y_{lm}(\theta,\phi)\left[\sum_{J=1}^{\infty}\frac{2\pi\mu}{\sqrt{k_ak_b}}M_{J,l}(k_a,k_b)(2J+1)\left[\frac{\pi\kappa c}{V}\right]^{1/2}e^{i\delta_J(b)}e^{i\delta_J(a)}i^{J+1-l}\times\epsilon_{\kappa\alpha}(m)\sqrt{(2l+1)4\pi}\begin{pmatrix}l&J&1\\m&0&-m\end{pmatrix}\begin{pmatrix}l&J&1\\0&0&0\end{pmatrix}\right]\ . \tag{11b}$$

In the summation, m is restricted to the values $0,\pm1$ and $\epsilon_{\kappa\alpha}(m)$ is the mth component of the spherical tensor of rank one, J is restricted to odd integers, and

$$M_{l,l'}(k_a,k_b)\equiv\frac{1}{\sqrt{k_ak_b}}\int_0^\infty dR\, s_l(k_aR)D(R)f_{l'}(k_bR)\ . \tag{11c}$$

The cross section for the collision-induced transition $\mathrm{He}(2\,^1S)+\mathrm{He}(1\,^1S)\rightarrow\mathrm{He}(1\,^1S)+\mathrm{He}(1\,^1S)+\hbar\omega$ is obtained by summing $|f_{\kappa\alpha}(\theta,\phi)|^2$ over all final states that conserve energy with the initial state, and dividing the result by the flux in the incident channel. The $\mathrm{He}(2\,^1S)+\mathrm{He}(1\,^1S)$ channel is a linear combination of the $A\,^1\Sigma_u^+$ and $C\,^1\Sigma_g^+$ states; since the excited gerade state is not allowed to make a radiative transition to the gerade ground state, the flux in the incident channel is twice the flux in the $A\,^1\Sigma_u^+$ channel.

We get

$$\sigma=\sum_\alpha\int\frac{d^3\kappa}{(2\pi)^3}\frac{V}{2\mu k_a}\int d^3k_b\,\delta\left[\frac{k_b^2}{2\mu}-\frac{k_a^2}{2\mu}+\Delta E-\hbar\omega\right]|f_{\kappa\alpha}(\theta,\phi)|^2=\int^{\omega_{\max}}d\omega\frac{d\sigma}{d\omega}\ ,$$

where

$$\frac{d\sigma}{d\omega}=\frac{8}{3}\left[\frac{\pi\mu}{k_a}\right]^2\frac{1}{c^3}\omega^3\sum_J\left[JM^2_{J,J-1}(k_a,k_b)+(J+1)M^2_{J,J+1}(k_a,k_b)\right], \tag{12}$$

ΔE is the energy defect of the transition at $R=\infty$, and $\omega_{\max}$ is the maximum angular frequency of the emitted photon. In deriving (12) we have used the continuum limit for the sum over photon states, $\sum_{\kappa\alpha}\rightarrow(V/8\pi^3)\sum_\alpha\int d^3\kappa$. Expression (12) is identical to that obtained from the Fermi Golden Rule.[10] Equation (12) provides the spectrum, $d\sigma/d\omega$, of the emitted radiation, in addition to the total transition cross section.

An approximation that does not require an integration over the total spectrum is the optical-potential, or opacity, method. We derive it by first inserting the expression (6) for the amplitude $F_{\kappa\alpha}(\mathbf{R})$ into Eq. (5a) to get an integrodifferential eigenvalue equation for the amplitude $F_a(\mathbf{R})$

$$\left[\frac{-1}{2\mu}\nabla^2_R+V_a(R)-E\right]F_a(\mathbf{R})=\sum_{\kappa\alpha}\int d^3R'G^+(\mathbf{R}\mathbf{R}')U^\dagger_{\kappa\alpha}(\mathbf{R}')U_{\kappa\alpha}(\mathbf{R})F_a(\mathbf{R}'). \tag{13}$$

The right-hand side of (13) contains a complex, nonlocal potential, $V(\mathbf{R},\mathbf{R}')\equiv\sum_{\kappa\alpha}G^+(\mathbf{R},\mathbf{R}')U^\dagger_{\kappa\alpha}(\mathbf{R}')U_{\kappa\alpha}(\mathbf{R})$ that arises because of the interaction of the electrons with the vacuum. The real part of the potential induces a shift in the eigenvalue $V_a(R)$. Since the electron-radiation coupling is weak, this shift is very small and we ignore the real part of $V(\mathbf{R},\mathbf{R}')$ in (13). The imaginary part of $V(\mathbf{R},\mathbf{R}')$ is an absorptive potential, occurring because the excited electronic state can emit a photon and decay to the ground state. We call it the optical potential. Its presence introduces a complex phase shift in the elastic scattering solutions of (13) and the quenching cross section can be expressed in terms of the imaginary part of the complex phase shift. However, the optical potential is nonlocal. In calculations using the optical potential method,[11] it has been replaced by a local potential by introducing an approximation which is essentially classical, as we now demonstrate.

Because the term $U^\dagger_{\kappa,\alpha}(\mathbf{R}')U_{\kappa,\alpha}(\mathbf{R})$ appearing in (13) is real, the optical potential is proportional to the imaginary part of the retarded Green's function, which can be expressed as

$$\mathrm{Im}G^+(\mathbf{R},\mathbf{R}')=\pi\sum_{l=0}^{\infty}\sum_{m=-l}^{m=l}Y_{lm}(\theta,\phi)Y^*_{lm}(\theta',\phi')\int_0^\infty dk\,\delta\left[\frac{k^2}{2\mu}-\frac{k_a^2}{2\mu}+\hbar\omega-\Delta E\right]\frac{f_l(kR)f_l(kR')}{RR'}. \tag{14}$$

This result is obtained by using a spectral representation for the retarded Green's function and the identity $1/(x+i\epsilon)\rightarrow P/x-i\pi\delta(x)$ as $\epsilon\rightarrow0$. Using (14) we obtain for the nonlocal optical potential

$$V_{\mathrm{opt}}(\mathbf{R},\mathbf{R}')=\frac{i}{4\pi}\sum_\alpha\int d\Omega_\kappa\int_0^{k_{\max}}dk\sum_{l=0}^{\infty}\sum_{m=-l}^{m=l}Y_{lm}(\theta,\phi)Y^*_{lm}(\theta',\phi')\times\frac{\omega^3(k)}{c^3}\frac{f_l(kR)f_l(kR')}{RR'}D(R)D(R')(\hat{\mathbf{R}}\cdot\epsilon_{\kappa\alpha})(\hat{\mathbf{R}}'\cdot\epsilon_{\kappa\alpha}), \tag{15}$$

where $\omega(k)\equiv k_a^2/2\mu+\Delta E-k^2/2\mu$. In order to construct a local potential we now make the semiclassical approximation that the values of k that give the largest contribution in (15) are given by $k^2/2\mu\approx\Delta E+k_a^2/2\mu+V_b(r)-V_a(r)$. The frequency term $\omega^3=|\Delta E(R)|^3$ can now be taken outside the k integral. Using the completeness property of the radial function $f_l(kR)$ and the identity

$$\sum_{l=0}^{\infty}\sum_{m=-l}^{m=l}Y_{lm}(\theta,\phi)Y^*_{lm}(\theta',\phi')\frac{\delta(R-R')}{RR'}=\delta^3(\mathbf{R}-\mathbf{R}') \tag{16}$$

we get

$$V_{\mathrm{opt}}(\mathbf{R},\mathbf{R}')\approx\frac{i}{2}\delta^3(\mathbf{R}-\mathbf{R}')A(R),\qquad A(R)=\tfrac{4}{3}D^2(R)\frac{|\Delta E(R)|^3}{c^3}, \tag{17}$$

and Eq. (13) becomes

$$\left[\frac{-1}{2\mu}\nabla^2_R+V_a(R)-E\right]F_\alpha(\mathbf{R})=\frac{i}{2}A(R)F_a(\mathbf{R}). \tag{18}$$

The optical potential, in the form given in (18), has been used extensively in previous studies of radiative charge transfer processes.[11]

The cross section for the radiative quenching is given by[11]

$$\sigma=\frac{\pi}{k_a^2}\sum_J^\infty(2J+1)[1-\exp(-4\eta_J)], \tag{19}$$

where η_J is the imaginary component of the phase shift of the Jth partial wave of the solution to (18). The sum over J is restricted to odd integers. Because the right-hand side of (18) is small, we can use the distorted-wave approximation to obtain an expression for the phase shift η_J:

$$\eta_J=\frac{\pi\mu}{2k_a}\int_0^\infty dR\,|s_J(k_aR)|^2A(R). \tag{20}$$

Replacing the sum (19) by an integral, $s_J(k_a R)$ in (20), using the JWKB approximation to it, and recognizing that η_J is small, we obtain the semiclassical cross section

$$\sigma = 2\pi \left[\frac{2\mu}{E}\right]^{1/2} \times \int p\, dp \int_{R_c}^{\infty} dR \frac{A(R)}{[1 - V_a(R)/E - p^2/R^2]^{1/2}} , \tag{21}$$

where R_c is the classical turning point and E is the kinetic energy. Expression (21) was used in the calculation by Browne, Allison, and Dalgarno.[2]

III. POTENTIAL CURVES AND DIPOLE MOMENT

The calculation for the quenching cross sections requires accurate potential curves of the $X\,^1\Sigma_u^+$ and $A\,^1\Sigma_u^+$ electronic states of the He_2 molecule. With the exception of a shallow van der Waals minimum, the $X\,^1\Sigma_g^+$ ground state is repulsive. For it we adopt the potential curve used by Sando and Dalgarno[6] in their study of the absorption spectrum for 600-Å photons by thermal helium atoms. The potential curve for the $A\,^1\Sigma_u^+$ excited state exhibits a repulsive hump at a nuclear separation of approximately 3.1 Å, and for nuclear separations less than 3 Å it contains an attractive well with a depth of ≈ 2.5 eV. In addition to the bound states supported by the well, the potential barrier at 3.1 Å give rise to numerous quasibound levels. These quasibound levels are responsible for the rich structure seen in the absorption spectrum of He gas at thermal temperatures.[3] This hump was first predicted, theoretically, by Buckingham and Dalgarno[12] and later, by additional calculations carried out by Allison, Browne, and Dalgarno,[2] who obtained a barrier height of 0.084 eV at an internuclear separation of 3.17 Å. A more refined *ab initio* calculation for the $A\,^1\Sigma_u^+$ state was performed by Guberman and Goddard[4] who obtained a barrier height of 0.0607 eV at an internuclear separation of 3.09 Å. More recently, *ab initio* calculations using a multiconfiguration self-consistent central field method were carried out by Sunil *et al.*[5] for He_2 potential energy curves including the $A\,^1\Sigma_u^+$ state. They obtained a barrier height of 0.058 eV at an internuclear separation of 3.09 Å, a value which is consistent with the calculation of Guberman and Goddard.

In studying the absorption of 600-Å photons by a low-temperature helium gas, Sando and Dalgarno[6] derived a semiempirical potential curve of the $A\,^1\Sigma_u^+$ state valid in the range of internuclear separations between 2 and 3 Å. Their absorption data analysis led to a potential barrier of 0.049 eV which is about 0.011 eV smaller than the *ab initio* calculations mentioned above. Semiempirical potential curves of the $A\,^1\Sigma_u^+$ were derived by Brutschy and Halberland[7] using data from high-resolution differential cross section measurements of the elastic scattering of He with $He(2\,^1S, 2\,^3S)$. Their analysis led to a barrier height of 0.047 eV with an accuracy of $+0.002$ eV, -0.001 eV at $R = 3.1 \pm 0.05$ Å. Most recently, semiempirical potential curves of the $A\,^1\Sigma_u^+$ state were constructed by Jordan and Siska[8] based on an analysis combining scattering and spectroscopic data with *ab initio* theory. Their analysis arrived at a barrier height of 0.0502 ± 0.001 eV at $R = 3.132 \pm 0.02$ Å.

Because of the persistent discrepancy of about 0.01 eV for the barrier height between the *ab initio* and semiempirical calculations, we have calculated the quenching cross sections of (1) using both *ab initio,* and semiempirical potential curves for the $A\,^1\Sigma_u^+$ state. In Fig. 1 we compare the various potential curves for the $A\,^1\Sigma_u^+$ state in the region of internuclear $1a_0 < R < 10a_0$.

The transition dipole moment connecting the $A\,^1\Sigma_u^+$ and $X\,^1\Sigma_g^+$ state was calculated by Allison, Browne, and Dalgarno[2] using both a length and velocity formulation. At nuclear separations less than $5a_0$ the two formulations give different values for the dipole moment and the calculated dipole moment is unreliable in this region. This uncertainty in the dipole moment, at small internuclear distances, translates into uncertain quenching cross sections of process (1) at higher collision energies. Sando[10] used a

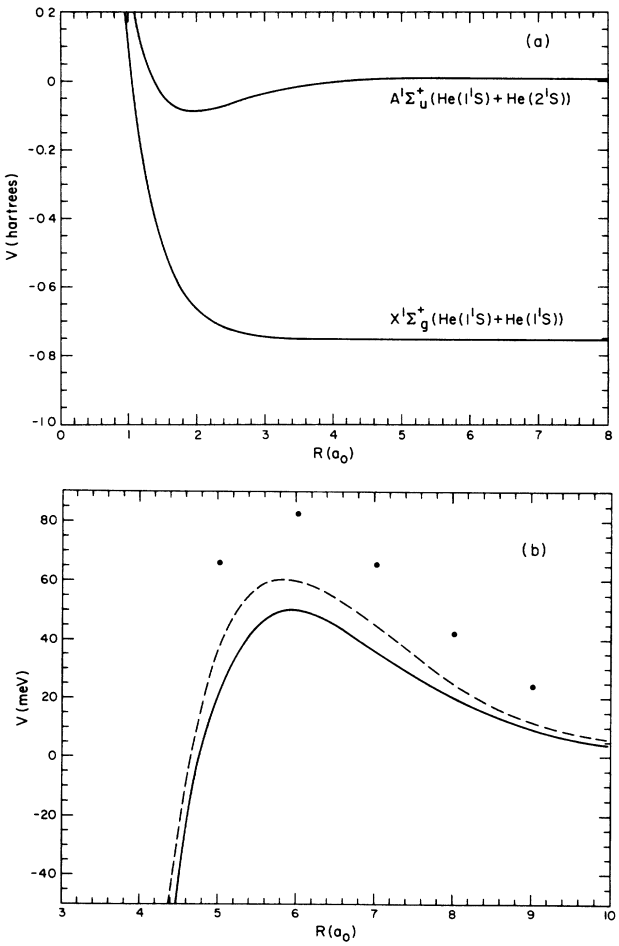

FIG. 1. (a) Potential energy curves of the $A\,^1\Sigma_u^+$ and $X\,^1\Sigma_g^+$ states of the He_2 molecule. The $A\,^1\Sigma_u^+$ potential is taken from Ref. 8 and the $X\,^1\Sigma_g^+$ ground state is taken from Ref. 6. (b) Repulsive hump in the $A\,^1\Sigma_u^+$ state. Solid circles are *ab initio* calculations of Allison, Browne, and Dalgarno (Ref. 2). The dashed line is the *ab initio* calculation of Guberman and Goddard (Ref. 4), and the solid line is the semiempirical result of Jordan and Siska (Ref. 8).

dipole moment that is an average of the values obtained from the length and velocity formulations, given in Ref. 4, and adjusted it so that the dipole moment converges to the united atom value. We use a dipole moment that has the correct united atom limit, and for distances between $1a_0$ and $9a_0$ we use a cubic spline fit to the length formulation values obtained in Ref. 2. For separations greater than $9a_0$, we fit the dipole moment to an exponential form $D(R)=11.65\exp(-0.639R)$. However, in order to assess the effect of the uncertainty of the dipole moment on the quenching cross sections, we have also carried out calculations using the values obtained from the hybrid formulation of Sando.[10] We find that the hybrid formulation dipole moment gives a quenching cross section, for thermal collisions, different from the above form by no more than 15%.

IV. RESULTS AND DISCUSSION

In Fig. 2(a) we plot the calculated cross sections for process (1). In this figure the cross sections are obtained using the optical-potential (OP) model, and are given in the collision energy range from 20 to 120 meV. At low collision velocities the He(2 ^1S)+He(1 ^1S) system does not have enough kinetic energy to penetrate the potential barrier of the $A\ ^1\Sigma_u^+$ state, and the quenching transitions occur in the region of internuclear separation greater than 3.1 Å. Above collision energies of 50 meV the system penetrates the potential barrier and samples regions where the $A\ ^1\Sigma_u^+$ state contains a deep attractive well. In this region there is a sharp rise in the cross sections and numerous resonances appear which are due to quasibound rotational-vibrational states of the He_2 molecule in the $A\ ^1\Sigma_u^+$ electronic state. In this figure we also plot the results obtained with the semiclassical approximation. At collision energies greater than 45 meV the semiclassical approximation gives somewhat smaller cross sections than the optical potential model, and it does not provide an accurate description of the resonances. At collision energies below 40 meV the semiclassical approximation agrees well with the cross sections obtained using the optical-potential (OP) approximation. In this energy range the transitions occur at nuclear separations greater than 3.1 Å, a region where the energy defect between the $A\ ^1\Sigma_u^+$ and $X\ ^1\Sigma_g^+$ is almost constant, and the semiclassical method provides a good approximation. In Fig. 2(b) we present the quantum distorted-wave method (QM) cross sections of (1), and we compare them to the cross sections obtained using the OP model. In obtaining the QM cross sections we have integrated, in (12), only over the part of the photon spectrum near 600 Å.

In Fig. 3 we present the calculated spectra, using Eq. (12), of the photons emitted by process (1) at the relative collision energies of 51.95 and 90 meV. At a collision energy of 51.95 meV there is a resonance in the cross section due to the presence of the rovibrational ($v=16$, $J=11$) quasibound state in the $A\ ^1\Sigma_u^+$ electronic state. The spectrum of the $J=11$ partial wave is compared, in Fig. 3(a), to the spectrum obtained by summing the contributions coming from all partial waves with $J<11$. It is clear from this figure that the majority of the emitted 600-Å photons, at this collision energy, arise from the resonance $J=11$ partial waves. In Fig. 3(b) the total spectrum of all partial-wave contributions, up to $J=23$, for a collision energy of 90 meV is presented. In both Figs. 3(a) and 3(b) the photon spectrum peaks in the vicinity near 600 Å, a property that is consistent with previous studies of the $^4He_2$ spectrum.[3] Using the semiclassical assumption that the frequency of the emitted photon is equal to the energy difference between the $A\ ^1\Sigma_u^+$ and $X\ ^1\Sigma_g^+$ states at the internuclear distance where the radiative transition occurs, we conclude that the 600-Å photon peak is due to the large probability for the system to un-

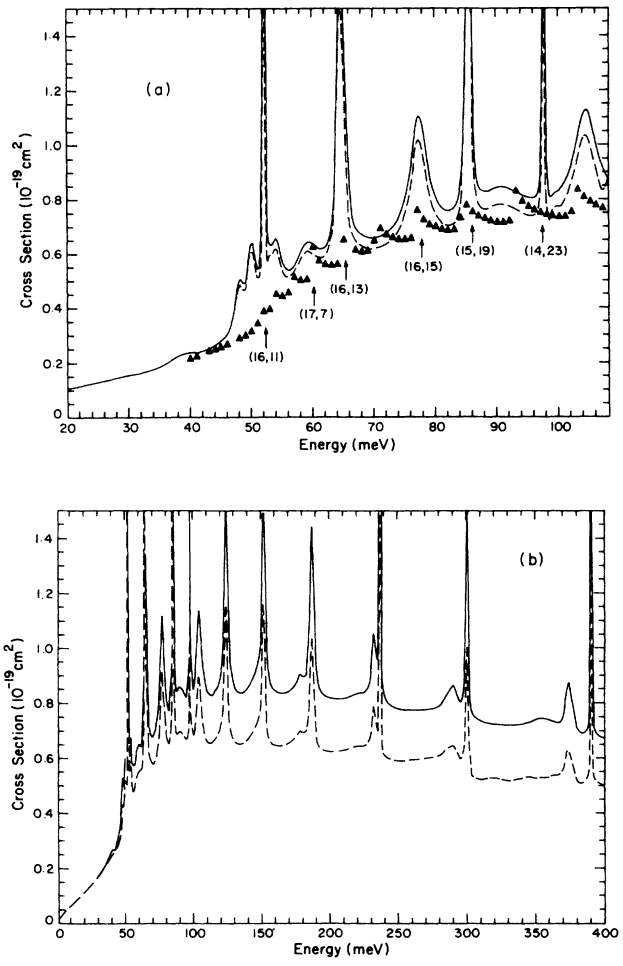

FIG. 2. (a) Cross sections for process (1). The solid line is the result using the length formulation radial dipole moment and the dotted line the result using the hybrid dipole moment. The cross sections correspond to the optical-potential expression (19). The triangles are the results obtained using the semiclassical approximation. The resonances are labeled by the quantum numbers (v,J), where v is the vibrational quantum number and J is the rotational quantum number. (b) Comparison between the total quenching cross sections obtained using the optical potential (solid line) approximation, and the quenching cross sections with the emission of $\approx$600-Å photons obtained using the quantum-mechanical method (dashed line), given by Eq. (12).

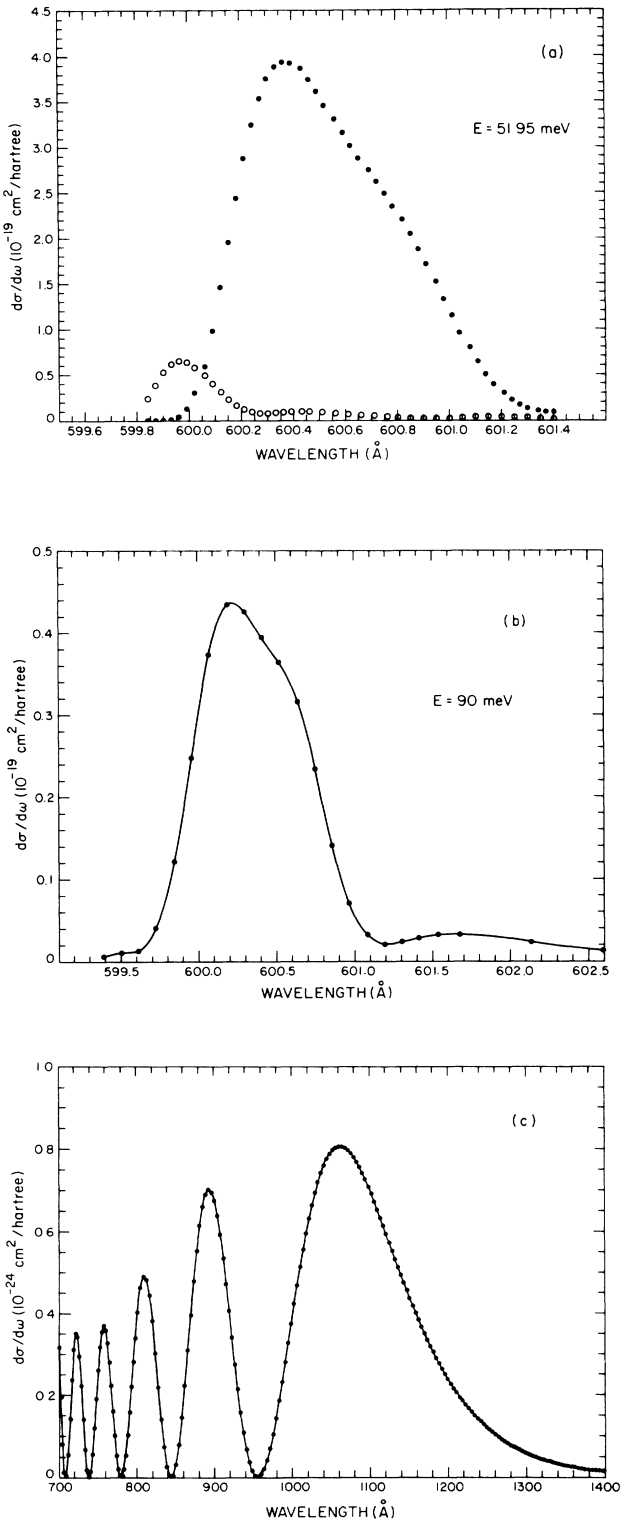

FIG. 3. (a) The solid points comprise the short-wavelength spectrum of the radiation emitted by process (1) from the ($v=16$, $J=11$) quasibound state of the $A\,^1\Sigma_u^+$ electronic state; the open circles comprise the spectrum contributed by all partial waves up to $J=11$. The relative collision energy is 51.95 meV. (b) The total spectrum, for short wavelengths up to partial wave $J=27$, emitted at a collision energy of 90 meV. (c) The long-wavelength spectrum for the $J=1$ partial cross section.

TABLE I. Spectral contributions to the partial cross sections, in units of 10^{-21} cm^2, for process (1). The first column tabulates the angular momentum J. The second column contains all contributions σ_A that result in the emission of photons with wavelength $\lambda < 610$ Å. The third column tabulates the contribution σ_B of the photons with 610 Å $< \lambda <$ 1400 Å, the fourth column is the sum of these contributions σ_T, and the fifth column is the cross section σ_{OP} obtained using the OP method. The collision energy is 90 meV.

J	σ_A	σ_B	σ_T	σ_{OP}
1	0.485	0.248	0.733	0.735
15	6.06	1.98	8.04	8.10
21	4.61	0.002	4.61	4.62

dergo a transition near the region where the $A\,^1\Sigma_u^+$ state has a maximum, at around 3.13 Å. If the system has enough kinetic energy to penetrate the barrier then there will also be a finite probability that the transitions can occur at smaller internuclear distances.

In Fig. 3(c) we present the spectrum for wavelength region between 700 and 1400 Å, emitted by the $J=1$ partial wave at a collision velocity of 90 meV. This, longer wavelength, region corresponds to transitions occurring near the inner wall of the $A\,^1\Sigma_u^+$ potential curve. We see a large, wide, peak in the spectrum at 1050 Å and considerable oscillatory structure in the 700–1000-Å region. Although the density, $d\sigma/d\omega$ is orders of magnitudes less than the corresponding density for the 600-Å photons, these photons contribute significantly to the overall quenching cross section (1) as is illustrated in Table I, in which we compare values for the partial cross sections of (1) at a collision energy of 90 meV. In the second column we present the contribution to the quenching cross section resulting in the emission of photons near 600 Å, and in the third column the contribution resulting in the emission of all other photons, most of which come from the 800–1400-Å region. Their sum represents the total quenching cross section and is given in the fourth column. These cross sections are in very good agreement with the total cross sections obtained using the OP method (fifth column). The partial cross sections for the $J=1$ and 15 partial waves contain a significant contribution coming from the region where the longer-wavelength photons are emitted. However, for the partial wave with $J=21$ most of the contribution comes from the 600-Å photons. This is understood by noticing that the classical turning point for $J=21$ is near the region where the potential curve for the $A\,^1\Sigma_u^+$ state has a maximum at 3.13 Å. The incoming He($2\,^1S$)+He($1\,^1S$) system now has a much smaller probability of reaching the inner region where the potential curve of the $A\,^1\Sigma_u^+$ state is repulsive and where the longer-wavelength photons are emitted.

The disparity between the OP cross section and the QM cross sections presented in Fig. 2(b) is thus a result of omitting the 800–1400-Å photon contribution when integrating over the spectrum in (12). From Fig. 2(b) we observe that as much of 20–25 % of the total quenching cross sections is due to this contribution at higher collision velocities. In Fig. 4, we present the partial cross

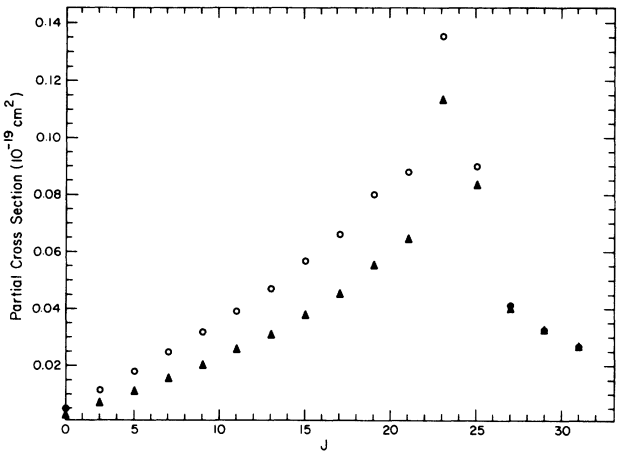

FIG. 4. Comparison between partial cross sections for the quenching cross section (1) with the emission of 600-Å photons obtained using the quantum-mechanical expression Eq. (12) (triangles) and the partial cross sections obtained using the optical-potential approximation (open circles). The collision energy is 120 meV.

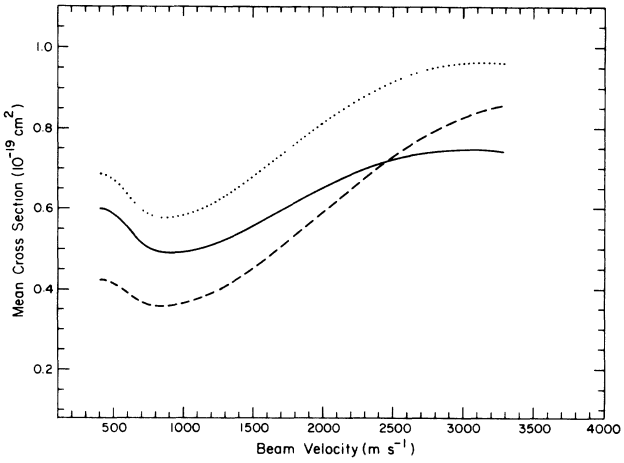

FIG. 5. Thermal-averaged cross sections for process (1) at a cell temperature of 300 K. The dotted line is the results for the total effective cross sections. The solid line is the effective cross sections for (1) with the emission of 600-Å photons. Both results use the semiempirical potential curve for the $A\ ^1\Sigma_u^+$ state given by Jordan and Siska (Ref. 8). The dashed line is the total quenching cross sections obtained by using the *ab initio* potential given by Guberman and Goddard (Ref. 4).

sections of (1) for a collision energy of 120 meV as a function of the total angular momentum J of the system, and we compare the partial cross sections obtained by the OP and QM theories. Again, we have integrated over the spectrum where it peaks, near 600 Å, to obtain the QM value. The difference between the OP and QM cross sections, at lower values of J is due to the omission of the contributions coming from the longer-wavelength photons. For larger angular momenta the incoming system cannot penetrate the centrifugal barrier near 3.13 Å, and the integrated spectrum of the 600-Å photons then gives an identical value to the OP method total cross sections. In Table II we compare the rate coefficients for (1) given in Ref. 4 to the ones obtained by our calculation.

In a beam-cell experiment,[9] the rate coefficient can be expressed in the form of an effective cross section

$$\bar{\sigma} \equiv \frac{\langle v\sigma \rangle}{v_b} , \tag{22}$$

TABLE II. Rate coefficients of process (1), in units of 10^{-14} cm^3 s^{-1}, for ^{4}He in thermal equilibrium at temperature T (K). In the second column are values obtained in Ref. 4 [Allison, Browne, and Dalgarno (ABD)], in the third column are the results obtained using the optical potential (OP) approximation, and the potential curve for the $A\ ^1\Sigma_u^+$ state, given in Ref. 2. All results use the length dipole moment.

T	ABD	OP
250	0.14	0.68
500	0.56	1.59
1000	1.27	2.62
2000	1.99	3.44
4000	2.54	3.96
8000	2.90	4.23
16 000	3.10	4.32
32 000	3.20	4.32

where v_b is the speed of a beam of metastable atoms, and the target has a Boltzmann distribution of velocities. The theoretical values of $\bar{\sigma}$ are plotted in Fig. 5. The dotted line is the total effective cross section and was obtained by using the OP approximation. Because the experimental setup is designed to measure the emitted 600-Å photons in (1) we included the results for the effective cross sections with the emission of photons near 600 Å using the QM method given by (12). These results are plotted by the solid curve, and this effective cross section is about 20% smaller at higher beam velocities than the total effective cross section. Both results are obtained using the semiempirical curves of Jordan and Siska[8] for the $A\ ^1\Sigma_u^+$ state. The dashed line represents the OP approximation results obtained using the *ab initio* calculation potential curve of the $A\ ^1\Sigma_u^+$ state of Guberman and Goddard.[4] The *ab initio* potential curve has a slightly higher repulsive hump, by about 0.011 meV, than the semiempirical curve of Jordan and Siska. The cross sections are quite sensitive to the height of this hump, and the beam-cell averaged cross sections obtained using the *ab initio* potential curve of Guberman and Goddard are about 33% smaller at low beam velocities than the cross sections obtained using the semiempirical potential of Jordan and Siska.

The accuracy of the predicted cross sections is limited by uncertainties in the transition dipole moment. The accuracy is less at higher relative collision velocities for which the radiative transitions occur at smaller internuclear distances. An improved calculation of the dipole moment function would permit a precise prediction of the quenching cross sections and rate coefficients.

ACKNOWLEDGMENTS

We thank Dr. R. Feltgen for discussions about his experiments. He stimulated our interest in this problem. We also thank the National Center for Supercomputer Applications, University of Illinois at Urbana-Champaign for the use of their CRAY-XMP computer. This work was supported by the U.S. Department of Energy, Office of Basic Energy Sciences, Division of Chemical Sciences.

[1]A. V. Phelps, Phys. Rev. **99**, 1307 (1955); D. M. Bartell, G. S. Hurst, and E. B. Wagner, Phys. Rev. A **7**, 1068 (1973); M. G. Payne, G. S. Hurst, M. H. Nayfeh, J. P. Judish, C. H. Chen, E. B. Wagner, and J. P. Young, Phys. Rev. Lett. **35**, 1154 (1975).

[2]D. C. Allison, J. C. Browne, and A. Dalgarno, Proc. Phys. Soc. **89**, 41 (1966).

[3]J. L. Nickerson, Phys. Rev. **47**, 707 (1935); T. Lyman, Astrophys. J. **60**, 1 (1924); L. A. Sommer, Proc. Natl. Acad. Sci. **13**, 213 (1927); P. G. Kruger, Phys. Rev. **36**, 855 (1930); Y. Tanaka, Sci. Pap. Instrum. Phys. Chem. Res. Tokyo **39**, 465 (1942); Y. Tanaka and K. Yoshino, J. Chem. Phys. **39**, 3081 (1963).

[4]S. L. Guberman and W. A. Goddard III, Phys. Rev. A **12**, 1203 (1975); S. L. Guberman, Ph.D. dissertation, California Institute of Technology, 1973.

[5]K. K. Sunil, J. Lin, H. Siddiqui, P. E. Siska, and K. D. Jordan, J. Chem. Phys. **78**, 6190 (1983).

[6]K. M. Sando and A. Dalgarno, Mol. Phys. **20**, 104 (1971).

[7]B. Brutschy and H. Halberland, Phys. Rev. A **19**, 2232 (1979).

[8]R. M. Jordan and P. E. Siska, J. Chem. Phys. **80**, 5027 (1984).

[9]C. Dehnbostel, R. Felgten, and G. Hoffman (unpublished).

[10]K. M. Sando, Mol. Phys. **23**, 413 (1972); **21**, 439 (1971).

[11]B. W. West, N. F. Lane, and J. S. Cohen, Phys. Rev. A **26**, 3164 (1982), and references therein.

[12]R. A. Buckingham and A. Dalgarno, Proc. R. Soc. London, Ser. A **213**, 327 (1952).